J. Fluid Mech. (1986), *vol.* 167, *pp.* 285–308
Printed in Great Britain

On long nonlinear internal waves over slope–shelf topography

By KARL R. HELFRICH† AND W. K. MELVILLE
R. M. Parsons Laboratory, Massachusetts Institute of Technology, Cambridge, MA 02139, USA

(Received 29 March 1985 and in revised form 16 December 1985)

An experimental and theoretical study of the propagation and stability of long nonlinear internal waves over slope–shelf topography is presented. A generalized Korteweg–de Vries (KdV) equation, including the effects of nonlinearity, dispersion, dissipation and varying bottom topography, is formulated and solved numerically for single and rank-ordered pairs of solitary waves incident on the slope. The results of corresponding laboratory experiments in a salt-stratified system are reported. Very good agreement between theory and experiment is obtained for a range of stratifications, topography and incident-wave amplitudes. Significant disagreement is found in some cases if the effects of dissipation and higher-order (cubic) nonlinearity are not included in the theoretical model. Weak shearing and strong breaking (overturning) instabilities are observed and found to depend strongly on the incident-wave amplitude and the stratification on the shelf. In some cases the instability of the lowest-mode wave leads to the generation of a second-mode solitary wave. The application of these findings to the prediction and interpretation of field data is discussed.

1. Introduction

Numerous *in situ* and remote-sensing observations demonstrate the ubiquitous nature of long, first-mode internal waves in many of the world's marginal seas, straits and coastal waters (Fu & Holt 1982). As these waves propagate for long distances in water of varying depth the effects of dissipation and topography are important in determining wave evolution. In an earlier paper (Helfrich, Melville & Miles 1984) one aspect of this problem, the scattering of solitary waves in a two-layer system by a gradually varying change in depth, was investigated theoretically and numerically. In this paper the evolution and stability of long internal waves over bottom topography are examined further by a combination of laboratory experiments and theoretical modelling.

Observations of internal waves in regions where topography is expected to be important include the Andaman Sea measurements of Osborne & Burch (1980) and the Sulu Sea data of Apel & Holbrook (1983). Both showed large-amplitude waves (heights of 80–90 m and lengths of 2 km) propagating into shallower water. Halpern (1971) and Haury, Briscoe & Orr (1979) measured smaller-scale internal wave groups in the Massachusetts Bay. The waves were moving towards the Massachusetts coastline. Similar phenomena have been measured in lakes (Thorpe 1971).

The wave-generation process typically involves stratified tidal flow over an isolated topographic feature and has been extensively studied (Maxworthy 1979;

† Present address: Woods Hole Oceanographic Institution, Woods Hole, MA 02543, USA.

Farmer & Smith 1980). On the other hand, the fate of these waves away from the generation region is not well understood. Since waves are generally observed to propagate into regions of decreasing depth (Fu & Holt 1982) dissipation, reflection and stability may all be expected to influence wave evolution.

Haury *et al.* (1979) observed overturning instabilities in the Massachusetts Bay measurements in a region of slowly changing depth. The exact mechanism was not identified although a shear instability was suggested. Sandstrom & Elliott (1984) conducted a field study along similar lines on the Scotian Shelf and found that large-amplitude waves, presumably generated at the shelf break, were completely dissipated within a distance of 10–30 km inshore of the shelf break. Estimates of the local Richardson number gave values of less than 0.25 leading to the conclusion that shear instability led to the dissipation. In addition they concluded that boundary and interfacial shear were significant, though not large enough to explain all the observed dissipation. The Sulu Sea data also emphasize the need to consider the influence of wave damping on evolution (Liu, Apel & Holbrook 1984).

The evolution and stability of these waves over variable topography is a topic which has consequences for the coastal environment. Haury *et al.* (1979) and Pingree & Mardell (1981) discussed the effects of wave stability and breaking on vertical mixing. Internal wave breaking may be an effective mechanism for mixing nutrient-rich water from the bottom to the biologically active upper layer (Sandstrom & Elliott 1984). Additionally, instabilities may play a role in the transfer of tidal energy to the high-frequency portion of the energy spectrum. The measurements of Haurey *et al.* demonstrated that wave energy, originally tidal, could be transferred to the scale of turbulence by breaking. It is known that places such as the Andaman Sea, the Gulf of California and the north-west Australian shelf, where tidally generated waves are observed, are regions of significant tidal dissipation (Miller 1966). Waves incident on the coast have also been suggested as a mechanism for coastal seiche excitement at Palawan Island in the Sulu Sea and at Puerto Rico (Giese *et al.* 1982).

Most previous efforts to describe the evolution of these waves have employed Korteweg–de Vries (KdV) theory. Lee & Beardsley (1974) used it to describe the initial evolution, in constant depth, of waves observed in the Massachusetts Bay and Osborne & Burch (1980) use it to analyse the Andaman Sea observations. KdV theory assumes a balance between nonlinearity and dispersion parameterized by two non-dimensional variables

$$\alpha = \frac{a_0}{D}, \quad \beta = \left(\frac{D}{l}\right)^2, \tag{1.1a,b}$$

where a_0 is a wave-amplitude scale, D is the water depth and l is a wavelength scale. For this balance to occur the nonlinear parameter α and the dispersive parameter β must be of the same order of magnitude and small: $\beta = O(\alpha) \ll 1$.

The additional parameters associated with topography and dissipation are respectively

$$\lambda = \frac{l}{L}, \quad \gamma = \frac{\delta}{D} = \frac{(\nu l/c)^{\frac{1}{2}}}{D}, \tag{1.2a,b}$$

where L is the horizontal lengthscale of depth variation, δ is the boundary-layer height scale, c is the linear long-wave phase speed and ν is a representative kinematic viscosity (eddy viscosity for the field, molecular viscosity for the laboratory). The (almost) two-layer stratification is specified by

$$\epsilon = \frac{h_\rho}{D}, \quad \sigma = \frac{\Delta\rho}{\rho_0}, \tag{1.3a,b}$$

(*a*) Physical scales

Location	a_0	l	D	d_+	L	c	$\sigma = \frac{\Delta\rho}{\rho}$	$h\rho$	ν
Andaman Sea	−80 m	2000 m	1500 m	500 m	250 km	2 m/s	0.002	500 m	1–10 cm²/s (eddy viscosity)
Mass. Bay	−10 m	300 m	80 m	30 m	10 km	0.5 m/s	0.002	30 m	1–10 cm²/s (eddy viscosity)
Laboratory	−2 cm	100 cm	30 cm	10 cm	700 cm	15 cm/s	0.3	2 cm	0.01 cm²/s (molecular viscosity)

(*b*) Non-dimensional parameters

Location	$\alpha = \frac{a_0}{D}$	$\beta = \left(\frac{D}{l}\right)^2$	$\lambda = \frac{l}{L}$	$\gamma = \frac{\delta}{D} = \frac{(\nu l/c)^{\frac{1}{2}}}{D}$	$\epsilon = \frac{h\rho}{D}$
Andaman Sea	−0.053	0.56	0.008	$2–7 \times 10^{-4}$	0.3
Mass. Bay	−0.13	0.07	0.03	$3–10 \times 10^{-3}$	0.4
Laboratory	−0.07	0.09	0.14	9×10^{-3}	0.1

TABLE 1. Representative scales in the ocean and laboratory

and the ratio of the depths of the layers, where h_ρ is the scale height of the pycnocline, $\rho_\pm$ is the upper/lower layer density, ρ_0 is a reference density, and $\Delta\rho = \rho_- - \rho_+$. Here ϵ is the interface parameter and σ is the Boussinesq parameter. If $\epsilon \ll 1$ then the system is nearly two-layered.

Physical scales and the non-dimensional parameters typical of the Andaman Sea and Massachusetts Bay internal waves are listed in table 1, where $d_\pm$ is the scale depth of the upper/lower layer. A range of eddy-viscosity values from 1 to 10 cm²/s was used in the calculations. The assumption of weak nonlinearity is satisfied in both cases. In the Andaman Sea $\beta \neq O(\alpha)$; however, Segur & Hammack (1982) found from laboratory experiments that the KdV equation was valid for β as large as 10α. Table 1 also shows that the depth variations are slow, $\lambda \ll 1$. If $\lambda \gg \alpha, \beta$ topographic influences would dominate nonlinearity and dispersion. Similarly, $\gamma \ll 1$ so that the influence of viscosity is limited to a small region near the boundary.

KdV theory for internal waves incorporating slowly varying topography and dissipation has not previously been tested. There may be some parametric regions in which the theory is inadequate, such as for large λ when reflection becomes important or if instabilities not modelled by the theory develop. Madsen & Mei (1969) found good agreement between KdV theory without dissipation for surface waves over slope/shelf topography. However, the extrapolation of this conclusion to internal waves is not straightforward owing to possible interfacial instabilities and differences in the KdV equation for surface and internal waves.

To determine the validity of the KdV theory for variable depth a comparison of theoretical models with laboratory experiments over slope–shelf topography is presented. Table 1 lists the typical parameter values studied in the experiments. Similarity with the field examples is preserved if a representative value of eddy viscosity is used in the oceanic calculations. Thus, extrapolation of conclusions from the laboratory to the field should be possible.

The experiments focus primarily on the problem of an internal solitary wave propagating up a slope to a shallower region of constant depth. Although field

observations generally show groups of nonlinear waves, the usefulness of KdV theory is best tested in the simple case of a single incident wave. Some studies of multiple incoming waves will be discussed.

The experiments were conducted around the 'turning-point' problem. A solitary wave in a two-layer system is a wave of depression/elevation for $d_+/d_- \lesssim 1$. In an inviscid system if a solitary wave of depression propagates up a slope through a point where $d_+ = d_-$, it can no longer exist as a wave of depression. The incident wave scatters into a train of oscillatory waves from which one or more solitary waves of reversed polarity may emerge asymptotically (Helfrich *et al.* 1984). This behaviour is due to the coefficient of the quadratic nonlinear term in the KdV equation changing signs upon passing through the turning point. In the region of the turning point higher-order cubic nonlinearity becomes important (Miles 1979; Helfrich *et al.* 1984). Investigation of this topographic scattering should provide a good test of the KdV theory for internal waves over bottom topography.

In §2 the governing equation, including variable topography, boundary-layer damping, continuous stratification and cubic nonlinearity, is formulated. Section 3 contains a description of the experimental set-up and procedure. The theoretical model predictions for the continuous stratification and two-layer models are compared with the experimental data in §4. In §5 observed wave instabilities, second-mode wave generation and mixing are discussed. A discussion of the results and application to oceanic conditions is presented in §6.

2. Evolution equation

We wish to obtain an evolution equation for long nonlinear internal waves over slowly varying topography. We consider a continuously stratified system, with the two-layer limit resulting when $\epsilon \downarrow 0$. Cubic nonlinearity is included as the first correction when the coefficient of the quadratic term becomes small. In the continuously stratified case this occurs when the pycnocline is near mid-depth, a situation which *must* be encountered for shoaling topography.

In table 1 representative values of the non-dimensional parameters for both coastal ocean and laboratory situations support the following assumptions used in the formulation of the governing KdV equation. The nonlinear and dispersive parameters are assumed to be in balance: $\beta = O(\alpha) \ll 1$. The slope of the bottom topography is slow, $\lambda = O(\alpha)$, though the depth change relative to a reference depth D may be $O(1)$. Boundary damping is not dominant, $\gamma \leqslant O(\alpha)$, but is important in wave evolution over long distances. The Boussinesq parameter is small, $\sigma \ll 1$. Thus a rigid lid is assumed. The interface parameter ϵ is assumed to be $O(\alpha)$, although this assumption may be relaxed. A schematic of the problem system is shown in figure 1.

With these scaling assumptions the governing KdV equation for the wave amplitude $A(X, s)$, normalized by a_0, can be deduced from Grimshaw (1981) and the boundary-layer analysis of Kakutani & Matsuuchi (1975) and Miles (1976) to be, in non-dimensional form,

$$A\Lambda + \frac{\partial A}{\partial X} + \alpha_1 A \frac{\partial A}{\partial s} + \beta_1 \frac{\partial^3 A}{\partial s^3} = \delta_1 \int_{-\infty}^{\infty} \frac{\partial A}{\partial s'} \frac{1 - \operatorname{sgn}(s - s')}{|s - s'|^{\frac{1}{2}}} \, \mathrm{d}s', \tag{2.1}$$

where

$$\Lambda = \frac{\mathrm{d}}{\mathrm{d}X} (\tfrac{3}{2} \ln c + \tfrac{1}{2} \ln I_0), \tag{2.2a}$$

$$\alpha_1 = \frac{3}{2c} \frac{I_1}{I_0}, \quad \beta_1 = \frac{1}{2c^3} \frac{I_2}{I_0}, \tag{2.2b}$$

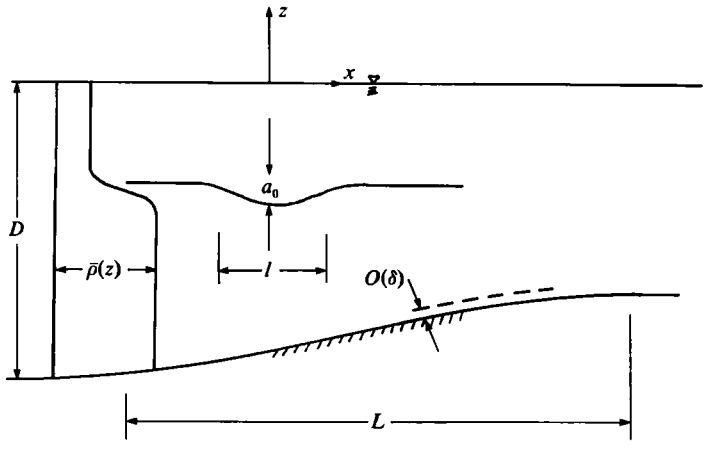

FIGURE 1. Definition sketch for continuously stratified system.

$$\delta_1 = \frac{(\gamma/\alpha)}{4\pi^{\frac{1}{2}} c I_0}\left[\left(2\frac{d_+}{W}\right)\bar{\rho}(0)\,\phi'(0)^2 + \left(1+\frac{2d_-}{W}\right)\bar{\rho}(-h)\,\phi'(-h)^2\right], \tag{2.2c}$$

and

$$I_0 = \int_{-h}^{0} \bar{\rho}\phi'^2\,\mathrm{d}z, \quad I_1 = \int_{-h}^{0} \bar{\rho}\phi'^3\,\mathrm{d}z, \quad I_2 = \int_{-h}^{0} \bar{\rho}\phi^2\,\mathrm{d}z. \tag{2.3a–c}$$

Here the horizontal and vertical coordinates (x, z) are normalized by (l, D), time t by l/U and mean density $\bar{\rho}(z)$ by ρ_0. The water depth h is a function of the slow spatial scale $X = \alpha x$ and phase variable,

$$s = \int_{x_0}^{x} \frac{\mathrm{d}x}{c} - t, \tag{2.4}$$

specifies rightward propagating disturbances. The vertical structure function $\phi(z; X)$ is found from the eigenvalue problem for the linear phase speed $c(X)$,

$$\frac{\partial}{\partial z}\left(\bar{\rho}(z)\frac{\partial \phi}{\partial z}\right) - \frac{1}{c^2}\bar{\rho}_z\phi = 0, \tag{2.5a}$$

$$\phi(0) = \phi(-h(X)) = 0. \tag{2.5b}$$

In order to compare predictions of the theory with laboratory data the coefficient for boundary damping (2.2*c*) has been modified to include dissipation due to the tank sidewalls by inclusion of the terms $2d_\pm/W$ where W is the tank width and $d_\pm$ is the dimensional depth of the upper/lower layer. This is a good approximation provided $\epsilon = h_\rho/D = O(\alpha)$. For $\epsilon = O(1)$ the horizontal velocity is not vertically uniform over most of each layer and (2.2*c*) would overestimate the sidewall influence. Since the difference between kinematic viscosity between fresh water and sea water is less than 3 % at 20 °C (Myers, Holm & McAllister 1969) an average value is used in (2.2*c*).

2.1. *Cubic nonlinear correction*

Under certain circumstances it is possible for the coefficient of the quadratic nonlinear term in (2.1), α_1, to become small. When the coefficient becomes $O(\alpha)$ the order of the entire quadratic term becomes $O(\alpha^2)$ and cubic nonlinearity, $O(\alpha^2)$, may balance or dominate quadratic nonlinearity in some parametric region (Miles 1979). The KdV

balance between nonlinearity and dispersion is lost in this equation. In the context of a two-layer system the appropriate balance is

$$\beta = O\left(\frac{|d_+ - d_-|}{D}\alpha\right).$$

If $|d_+ - d_-|/D = O(\alpha)$ then $\beta = O(\alpha^2)$ and cubic nonlinearity, which limits the maximum attainable wave height (Long 1956), should be incorporated into the theory.

The evolution equation corresponding to a two-layer system with slowly varying topography with $\beta = O(\alpha^2)$ and $\lambda = O(\beta)$ was derived by the multiple scales expansion method in Helfrich *et al.* (1984). The inclusion of the cubic nonlinear term for the case of continuous stratification is based on that derivation and Miles (1979, equation (5.6)). Thus, when $\beta = O(\alpha^2)$ the cubic nonlinear correction in the continuous case is $-(3I_3/cI_0)A^2A_s$ where

$$I_3 = \int_{-h}^{0} \bar{\rho}\phi'^4 \,\mathrm{d}z. \tag{2.6}$$

Gear & Grimshaw (1983, equation (84)) showed that (2.6) is not complete and should include another term. However, in the limit of a two-layer system this correction is identically zero and for continuous but thin interfaces, the leading behaviour is given by (2.6).

The effects of nonlinearity, dispersion, slowly varying topography and boundary damping all enter without interaction at the highest order resulting in the extended KdV equation (EKdV)

$$A\Lambda + \frac{\partial A}{\partial X} + \alpha_1 A\frac{\partial A}{\partial s} - \alpha_2 A^2\frac{\partial A}{\partial s} + \beta_1\frac{\partial^3 A}{\partial s^3} = \delta_1\int_{-\infty}^{\infty}\frac{\partial A}{\partial s'}\frac{1-\mathrm{sgn}\,(s-s')}{|s-s'|^{\frac{1}{2}}}\,\mathrm{d}s', \tag{2.7}$$

where

$$\alpha_2 = \frac{3I_3}{cI_0}, \tag{2.8}$$

and Λ, α_1, β_1, and δ_1 are given by (2.2).

For constant depth and no damping (2.7) has the solitary-wave solution (Miles 1979).

$$A = a_0(\cosh^2\theta - \mu\sinh^2\theta)^{-1},$$

where

$$\theta = \frac{x}{l}\left(1 - \frac{2}{l^2}\frac{I_2}{I_0}\right) - \frac{c}{l}t,$$

and $0 < \mu < 1$. For a given stratification, depth and wave amplitude, the wavelength scale l is found from

$$l^{-2} = \frac{1}{4}\frac{a_0}{I_2}(I_1 - a_0 I_3),$$

and μ is given by

$$\mu = \frac{1}{4}\frac{a_0^2 l^2}{D^3}\frac{I_3}{I_2}.$$

2.2. *Two-layer model*

In the limit of a two-layer system the coefficients of the EKdV equation (2.2*a–c*), and (2.8) become (Helfrich *et al.* 1984)

$$A = \frac{1}{2c}\frac{\mathrm{d}c}{\mathrm{d}X}, \tag{2.9a}$$

$$\alpha_1 = \frac{3}{2c}\frac{(d_+ - d_-)}{(d_+ d_-)}, \tag{2.9b}$$

$$\alpha_2 = \frac{3}{c}\frac{1}{(d_+ d_-)^2}\frac{(d_+^3 + d_-^3)}{(d_+ + d_-)}, \tag{2.9c}$$

$$\beta_1 = \frac{d_+ d_-}{6c^3}, \tag{2.9d}$$

and

$$\delta_1 = \frac{(\gamma/\alpha)}{4\pi^{\frac{1}{2}}c}\left(\frac{d_+ d_-}{d_+ + d_-}\right)\left[\frac{D}{W}\frac{2}{d_+} + \left(1 + \frac{D}{W}2d_-\right)\frac{1}{d_-^2} + \frac{1}{2}\left(\frac{d_+ + d_-}{d_+ d_-}\right)^2\right], \tag{2.9e}$$

where

$$c^2 = \sigma\frac{d_+ + d_-}{d_+ d_-}. \tag{2.10}$$

Here the layer depths $d_\pm$ are normalized by the total depth D at some reference location and the phase speed c is normalized by $U = (gD)^{\frac{1}{2}}$.

The third term in the brackets in (2.9*e*) explicitly accounts for interfacial damping and is found from an analysis similar to the bottom boundary layer (Helfrich 1984). For analytical tractability, the interface is assumed to be flat for the viscous boundary-layer problem. If this assumption is not made a fully nonlinear analysis results because the boundary-layer scale γ is comparable to the wave-amplitude scale α. The kinematic boundary condition applied at $z = \alpha A$ in the inviscid problem is applied at $\tilde{z} = (\alpha/\gamma)A \approx A$, where $A = O(1)$ in the non-dimensional formulation. Leone, Segur & Hammack (1982) made the same flat interface assumption when deriving a relationship for the adiabatic viscous decay of a solitary wave in a two-layer system.

2.3. *Numerical methods*

Equation (2.7) was solved using the explicit pseudospectral method of Fornberg & Whitham (1978). The vertical-structure eigenvalue problem (2.5*a, b*) was solved, using a fourth-order Runge–Kutta shooting technique, at several locations in order to determine the phase speed and the integrals I_j ($j = 0, 1, 2, 3$) as functions of x. Experimentally measured density profiles were used in the eigenvalue computations. Details of the numerical procedure can be found in Helfrich *et al.* (1984) and Helfrich (1984).

3. Experimental set-up and techniques

All experiments were conducted in a glass-walled wave tank 0.6 m high, 0.38 m wide and 24 m long (see figure 2). The straight slope and uniform shelf topography was constructed with a false bottom of removable plate-glass sections. Following Thorpe (1978) interfacial waves were generated with a flap-type wavemaker consisting of a 1.2 m Plexiglas flap hinged to an airfoil section fixed in the interface. Accurate and repeatable flap movement was attained using a computer-controlled stepper

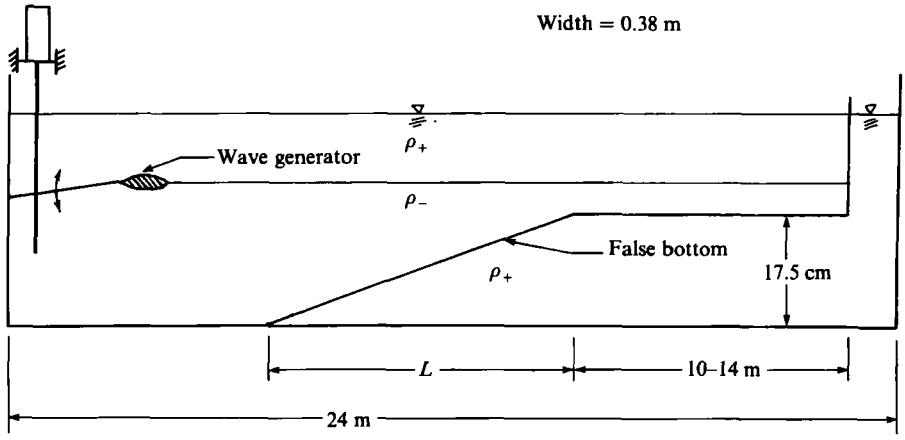

FIGURE 2. Experimental facility.

motor and threaded rod. Single and multiple solitary waves were generated by moving the flap such that the mass flux in each layer approximated that of a wave passing the tip of the airfoil (after Goring 1978). An LSI 11/23 microcomputer was used for experimental control and data acquisition.

A salt-stratified system was constructed by filling the tank to a pre-determined depth with salt water of known density and then slowly spreading fresh water over the salt water with floating diffusers. Precision Measurement Engineering microscale conductivity probes (Model 106), vertically positioned by computer-controlled stepper motors, were used to measure background-density profiles and interfacial displacements. Probes were usually located at the base of the slope and at several other locations on the slope and shelf.

Interfacial displacements were calculated assuming lowest-mode motion. The conductivity probes were positioned within the interfacial region prior to a run and measured conductivities (densities) were converted to equivalent vertical displacements of the static conductivity profile. A test of the accuracy of these measurements was made by comparing velocities calculated from measured displacement records with fluid velocities measured with a laser-Doppler anemometer. The calculated velocity at the laser measuring depth z_v is, from the linear problem,

$$u(t) = c\phi'(z_v)\, A(t),$$

where A is the measured dimensional interfacial displacement amplitude and c is the dimensional phase speed. The phase speed c and $\phi(z)$ are found by solving the eigenvalue problem (2.5a, b) with the measured static density profile. Figure 3 shows an example comparison for a scattered wave packet on the shelf. The laser data is unfiltered; thus, high-frequency noise is evident. Agreement is very good, indicating that the conductivity probes and lowest-mode analysis give reliable estimates of interfacial displacements. Uncertainty in displacement calculations was found to be less than 10% of measured wave heights.

All experiments with topography were designed so that a solitary wave of depression would propagate onto a shelf where the relative layer depths were reversed. The ratio of the layer depths on the shelf is given by

$$r = \frac{d_{-s}}{d_+}, \tag{3.1}$$

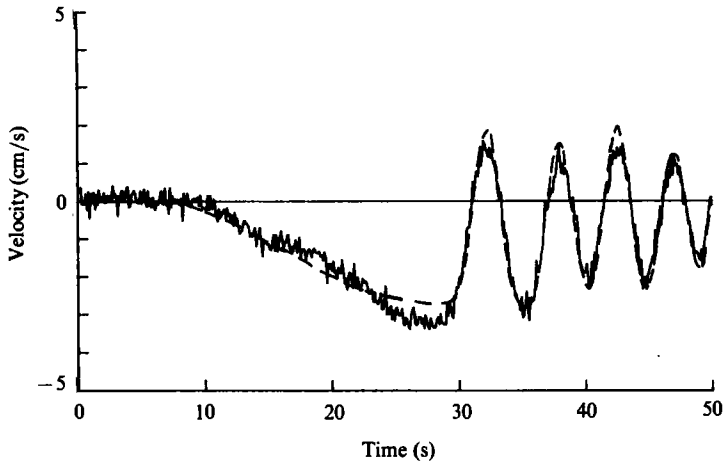

FIGURE 3. Comparison of velocity measured with laser anemometer (——) and velocity calculated from measured conductivities (– – –). Data from lower layer 2 m past shelf break.

(*a*) Dimensional parameters

a_0 (cm)	D (cm)	L (cm)	d_{-s} (cm)	d_+ (cm)	Δh (cm)	$h\rho$ (cm)
	33.5	244	5.0			
−1.4 to −2.5	35.0	488	6.5	11.0	17.5	1.7 to 3.0
	36.0	701	8.0			

(*b*) Non-dimensional parameters

α	λ	r	σ	ϵ
		0.45	0.017	
−0.03 to −0.075	0.1 to 0.33	0.59	0.035	0.05 to 0.1
		0.73	0.053	

TABLE 2. Ranges of parameters examined experimentally

where d_{-s} is the depth of the lower layer on the shelf. For $r < 1$ a turning point is encountered on the slope and as r decreases the topographic scattering of the incident wave increases.

Table 2 lists the wave amplitudes, water depths, topography and stratifications examined. For all runs the height of the slope, Δh, and the depth of the upper layer were constant. The interface thickness was essentially constant with a typical maximum slope thickness of 2 cm. The non-dimensional parameters α, λ, r and σ were varied systematically in order to examine their influence on wave evolution, stability and the theoretical modelling.

4. Comparison with experiments

Several runs were conducted at constant depth in order to test the boundary-layer-dissipation model. Figure 4 shows a comparison between the continuous stratification model (2.7) and experimental data for the evolution of a single solitary wave with $\alpha = -0.043$ and $(d_+, D, \sigma) = (11\text{ cm}, 33.5\text{ cm}, 0.0355)$. The non-dimensional

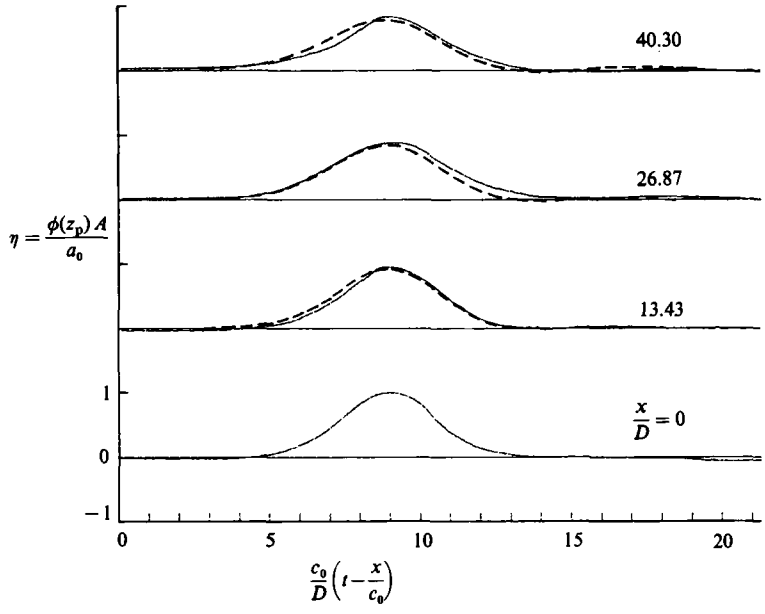

FIGURE 4. Model comparison for uniform depth. $(\alpha, D, d_+, c_0, \sigma) = (-0.043, 33.5\text{ cm}, 11\text{ cm}, 16.0\text{ cm/s}, 0.035)$. ——, experiment; – – –, theory.

streamline displacement $\eta = \phi(z_p)\,A/a_0$ at the probe depth z_p is plotted against the retarded time

$$t-\int_{x_0}^{x}\frac{\mathrm{d}x}{c}\quad\left(\text{normalized by }\frac{c_0}{D}\right)$$

for four locations in the tank. Data at the first probe location ($x_0 = 0$, 2.5 m from the tip of the wavemaker) was used to define a_0 and provided the initial data for the numerical calculations. In this and subsequent comparisons the sign of the wave amplitudes is contained in $\alpha = a_0/D$. Damping due to interfacial shear was accounted for by altering (2.2c) to include the two-layer interfacial damping formulation (cf. (2.9e)). The agreement between theory and experiment is very good in both amplitude and phase of the evolving wave. Comparisons without interfacial damping show an overestimate of wave amplitude by about 20% at $x/D = 40.3$. Leone *et al.* (1982) made the same approximation in examining the decay of solitary waves in a salt-stratified system. They observed significant differences between their measurements and predictions which they attributed to residual kinetic energy in the boundary layers from a freely propagating fast surface mode. The internal-wave-generation method used in this study is volume preserving and does not generate fast surface waves.

The steep front face of the experimental waveform shown at $x/D = 40.30$ is probably due to distortion of the conductivity (displacement) signal as heavy (salty) fluid drained down the vertically oriented conductivity-probe tip. Some L-shaped probes (probe tips enter the interface normal to the (x, z)-plane) were available ($x/D = 0$, 26.87) and helped reduce this problem.

Next, the continuous stratification model, employing the two-layer interfacial dissipation formulation, is compared with the experimental data. The comparisons are generally insensitive to σ, so only the data for $\sigma = 0.035$ will be examined. The

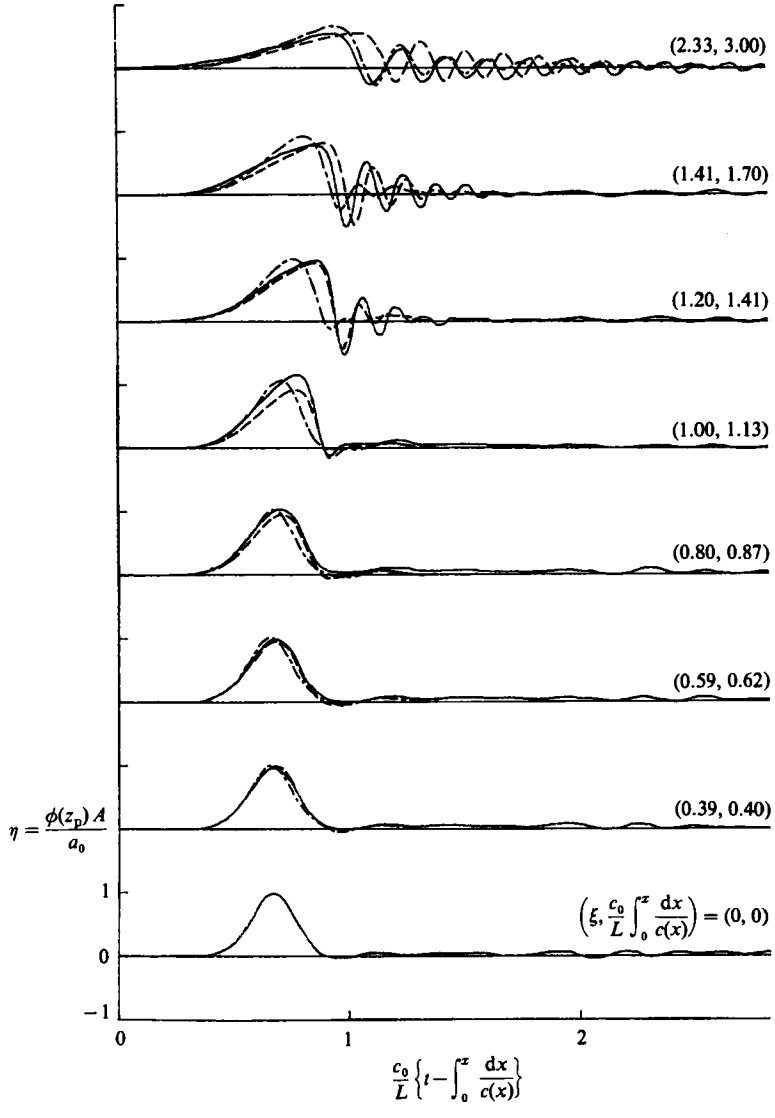

FIGURE 5. Extended KdV (– – –) and KdV (— — —) model comparison with composite of wave evolution over slope–shelf topography. $(\alpha, \lambda, r) = (-0.05, 0.15, 0.59)$ and $(L, D, d_{-s}, c_0, \sigma) = (488$ cm, 35 cm, 6.5 cm, 15.3 cm/s, 0.0336).

comparisons are plots of the streamline displacement $\eta = \phi(z_P)\, A/a_0$ vs. the retarded time normalized by c_0/L ($= -\lambda s$ in the notation of (2.7)) at several locations ($\xi \equiv x/L$) on the slope and shelf. In all examples the measured displacements at the slope base ($\xi = 0$) were used as the initial conditions for the numerical computations.

Figure 5 shows a comparison of the KdV theory with and without the cubic nonlinear term for $(\alpha, \lambda, r, \sigma) = (-0.055, 0.15, 0.59, 0.0336)$. This figure is a composite of experimental data from five successive runs since only four conductivity probes were available during a run. Wave generation using the computer-controlled stepper motor results in excellent repeatability of the incident wave thereby allowing a composite picture of wave evolution on the slope to be constructed. The agreement between the KdV equation and the data is poor for the measuring stations $\xi = 0.8$

to 1.41. Addition of the cubic term improves the predictions. In particular the predicted shape of the evolving wave on the slope and just on the shelf is much better using the extended equation. Errors in predicted amplitude using the extended theory are confined to the neighbourhood of $\xi = 1.0$ and are probably due to the abrupt slope change at the shelf break. Measured fluid velocities in this region (discussed in §5) are $O(c)$, which conflicts with the assumption of weak nonlinearity. At the last station ($\xi = 2.33$) the EKdV theory gives a larger error in phase than the KdV model, but does give a better prediction of wave amplitudes in the tail of the scattered packet.

The phase error is probably the result of retaining the higher-order cubic term in the model. Formally, other higher-order terms ($O(\alpha\beta, \beta^2)$) should also be retained in the model along with the cubic term outside the turning-point region. A sample calculation using the wave characteristics computed with the EKdV model at $\xi = 1.2$ showed that the modification to the linear two-layer phase speed from the $O(\beta^2)$ dispersive term (cf. Koop & Butler 1981, Appendix A) would correct most of the phase error at $\xi \equiv 2.33$. However, the influence of the $O(\alpha\beta)$ (mixed nonlinear-dispersive) terms might also be important but cannot be estimated easily. A test numerical run was made for the data of figure 5 using the EKdV model for the evolution on the slope ($0 \leqslant \xi \leqslant 1$) and then employing the results at $\xi = 1.0$ as the initial conditions for the KdV model on the shelf. The phase error at $\xi = 2.33$ was nearly eliminated and the amplitude and frequency predictions were very good. However, there is no *a priori* justification for this hybrid modelling.

The influence of slope length is examined in figure 6. Two comparisons are shown with the EKdV model for runs in which only the slope length was altered, other parameters were held essentially constant $(\alpha, r, \sigma) = (-0.04, 0.73, 0.355)$. Figure 6(*a*) is for the longest slope $(\lambda, L) = (0.12, 701$ cm) and shows good agreement at the two stations on the shelf. Figure 6(*b*) is for the shortest slope $(\lambda, L) = (0.33, 244$ cm). The agreement is excellent at both measuring stations even though $\lambda \approx 10\alpha$, considerably outside the assumed scaling. Note the small-amplitude shelf behind the incident wave at $\xi = 0$ in figure 6(*b*). The presence of weak reflection, not accounted for in the theory, does not noticeably affect the comparison. Typical maximum amplitudes of the reflected component are 5–10% of the incident-wave amplitude. The reflected component decreases as the slope length increases and is negligible for the long slopes (see figure 6*a*).

So far only experimental runs without strong wave instabilities have been considered. Figure 7 shows a comparison for $(\alpha, \lambda, r, \sigma) = (-0.063, 0.15, 0.45, 0.0356)$ in which wave breaking, accompanied by significant vertical mixing and generation of a second-mode solitary wave, occurred in a region $\pm l$ from the shelf break ($\xi = 1.0$). Details of the breaking events and second-mode generation are discussed in §5. Aside from the station at $\xi = 1.0$ the results are surprisingly good even though the weakly nonlinear theory cannot model any instabilities. Examination of measured velocities at the shelf break and velocities computed with measured displacement data indicates that the probe record is an accurate estimate of displacement. (The flat crest is a result of the interface being raised above the probe level.) At $\xi = 1.41$ the leading trough and first several wave crests are predicted accurately. Errors in amplitude and phase become significant at the rear of the scattered packet. This is a characteristic of other comparisons regardless of wave instabilities, and the error decreases as r increases.

Because of its simplicity, the two-layer model is often used as an approximation when studying long first-mode internal waves. Figure 8(*a*) shows a comparison of the two-layer model with experimental data for $(\alpha, \lambda, r, \sigma) = (-0.040, 0.15, 0.73, 0.0356)$.

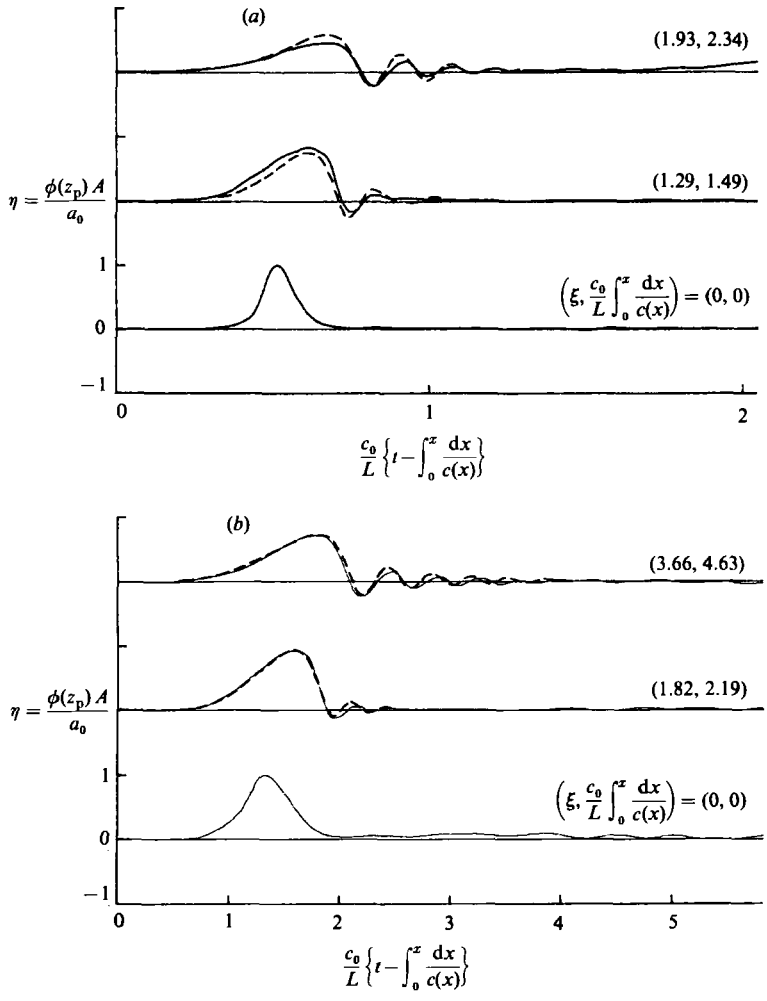

FIGURE 6. Model comparison for (*a*) long slope $(\lambda, L) = (0.12,\ 701\text{ cm})$ and (*b*) short slope $(\lambda, L) = (0.33,\ 244\text{ cm})$ with all other parameters held constant. $(\alpha, r) = (-0.04,\ 0.73)$ and $(D, d_{-s}, c_0, \sigma) = (36.5\text{ cm},\ 8.0\text{ cm},\ 15.9\text{ cm/s},\ 0.0355)$. ——, experiment; – – –, theory.

The model captures the qualitative aspects of the scattering process and is accurate in wave-amplitude prediction, though errors in phase and frequency are large. In particular the time for the leading trough to pass at $\xi = 1.41$ and 2.33 is not modelled accurately. Figure 8(*b*) shows the same experimental run compared with the continuous stratification model. The significant improvement with this model is attributable to differences in the linear phase speeds between the models. The two-layer model overpredicts phase speed by 3 % for $\xi \leqslant 0$ and 7 % for $\xi > 1$. Although these values are small, the cumulative effect on dispersion of the scattered waves over distances of 2–3 L is important.

Since most observations show rank-ordered groups of nonlinear waves several experiments were conducted with two rank-ordered waves to determine if the good agreement found for single waves applies to multiple waves. Figure 9 shows an example for two waves incident on the intermediate slope length and depth change with $(\alpha_1, \alpha_2, \lambda, r, \sigma) = (-0.055, -0.044, 0.15, 0.59, 0.0349)$. The overall agreement is

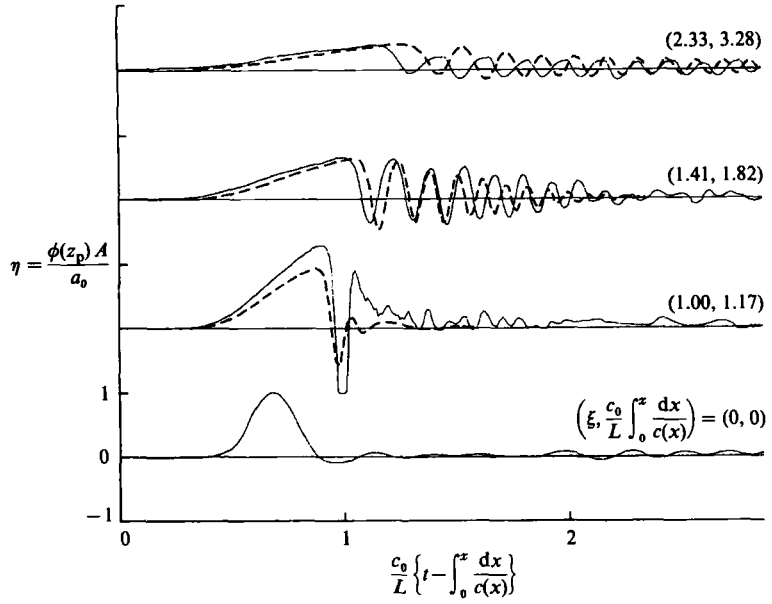

FIGURE 7. Model comparison for case with wave breaking at shelf break ($\xi = 1.0$). $(\alpha, \lambda, r) = (-0.063, 0.15, 0.45)$ and $(L, D, d_{-s}, c_0, \sigma) = (488$ cm, 33.5 cm, 5 cm, 15.5 cm/s, 0.0356). ——, experiment; – – –, theory.

very good. The largest errors, aside from the amplitudes at $\xi = 1.0$, are in the middle of the scattered packet at $\xi = 2.33$. In this region the scattered tail of the first wave is interacting with the front of the second wave. The disagreement is related to the errors in phase and amplitude in the tails of scattered packets for single incident waves. Numerical experiments for two rank-ordered waves propagating through a turning point (Helfrich *et al.* 1984) have demonstrated the importance of nonlinear interaction between scattered packets. Errors in modelling the tail of the lead wave will result in errors in modelling the interaction. Despite this error the agreement is quite good and improves as r increases.

5. Wave instabilities

Wave instabilities in the shelf-break region were observed under certain conditions. The instabilities ranged from interfacial shearing to strong wave breaking and overturning accompanied by significant horizontal and vertical mixing. Generation of a second-mode wave from this instability of the lowest mode occurred in some cases.

Figure 10 shows a series of shadowgraph images taken at the shelf break during a typical strong breaking event where $(\alpha, \lambda, r, \sigma) = (-0.067, 0.29, 0.45, 0.0530)$ and $(L, D, d_{-s}) = (244$ cm, 33.5 cm, 5 cm). The main features of the breaking events are not strongly dependent on slope length or density difference. In frame (*a*) the leading face of the incident wave (propagating from left to right) has elongated and moved onto the shelf. Steepening of the rear face is evident. In contrast to long surface waves, nonlinearity in this case tends to steepen the rear face. The nonlinear increase in the phase speed is proportional to $(d_+ - d_-)A$. Upon passing from a region where $d_+/d_- < 1$ to a region where $d_+/d_- > 1$, the effect of nonlinearity is to slow down the crest of the wave (incident wave has negative amplitude) relative to the front and

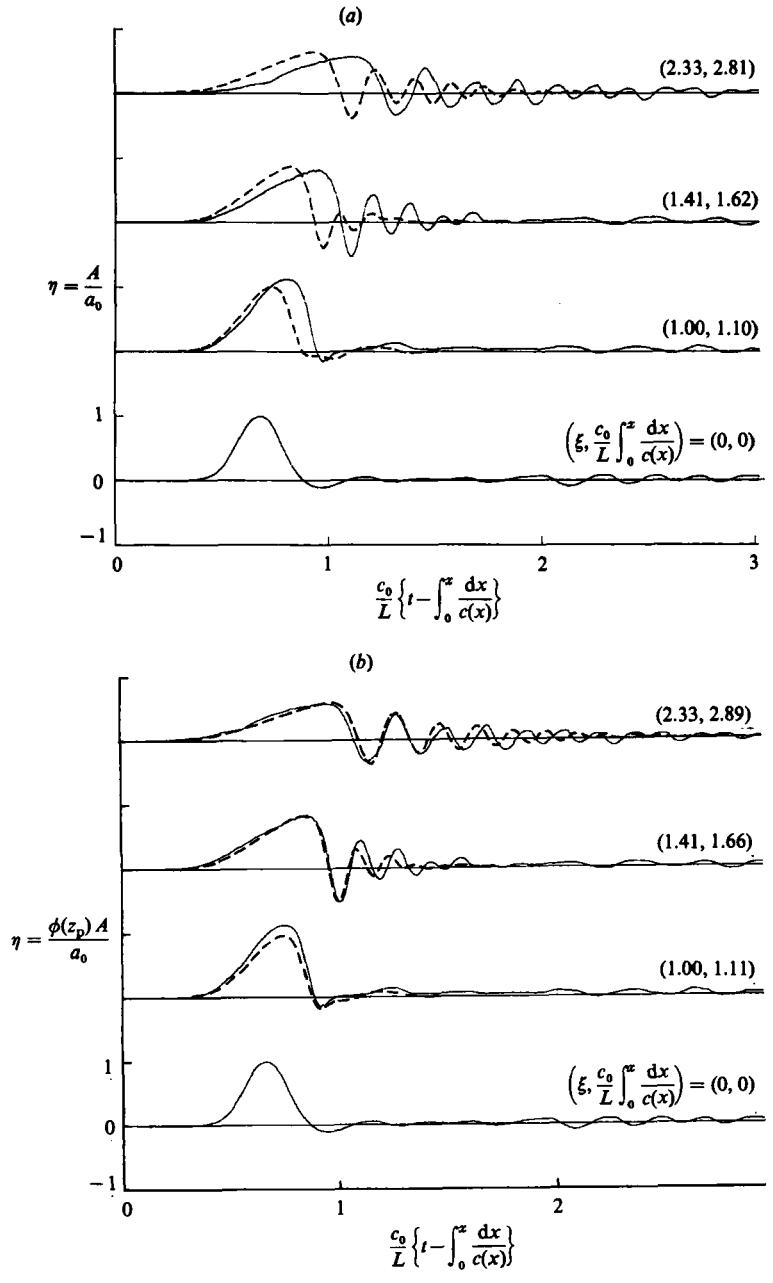

FIGURE 8. Comparison of (*a*) two-layer model and (*b*) continuous stratification model for same experimental run. $(\alpha, \lambda, r) = (-0.040, 0.17, 0.73)$ and $(L, D, d_{-8}, \sigma) = (488\text{ cm}, 36.5\text{ cm}, 8\text{ cm}, 0.0356)$. Two-layer $c_0 = 16.5$ cm/s and continuous $c_0 = 16.0$ cm/s. ——, experiment; – – –, theory.

rear faces, leading to steepening of the rear face. Slight mixing is evident on the rear face in frame (*a*). Note the sharp corner in frame (*c*) and the wave breaking and subsequent flow of mixed fluid down the slope in the following frame. Mixed fluid moves onto the shelf (frames (*e*) and (*f*)) and then collapses back on to itself (frames (*g*) and (*h*)). Mixed fluid moves further on the shelf in the form of a turbulent density intrusion.

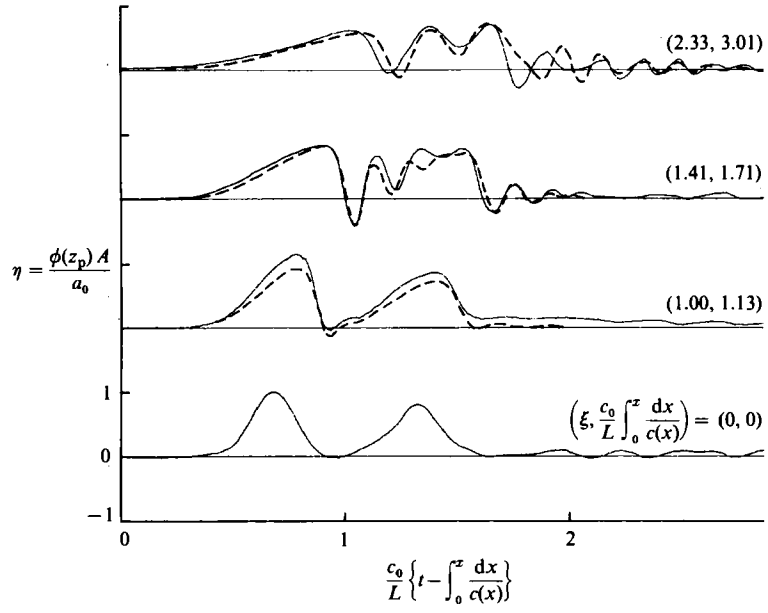

FIGURE 9. Model comparison for two rank-ordered solitary waves incident on slope-shelf topography. $(\alpha_1, \alpha_2, \lambda, r) = (-0.055, -0.044, 0.15, 0.59)$ and $(L, D, d_{-s}, c_0, \sigma) = (488$ cm, 35 cm, 6.5 cm, 15.5 cm/s, 0.0349). ——, experiment; – – –, theory.

The initial strong breaking event is two-dimensional with the resulting turbulence being clearly three-dimensional. Frame (*l*) shows the nearly horizontal striations typical of the decay of turbulent mixing events in stratified fluids (Pearson & Linden 1983). Their horizontal extent is $\sim \pm l$ from the shelf break.

The head of the turbulent intrusion (frames (*j*) and (*k*)) eventually propagates away from the mixing and forms what appears to be a second-mode solitary wave (Davis & Acrivos 1967; Benjamin 1967). These waves are characterized by an isolated varicose perturbation of the pycnocline and are long with respect to the interface thickness, but short compared with the total depth. Figure 11 shows a second-mode wave 45 cm past the shelf break for $(\alpha, \lambda, r, \sigma) = (-0.062, 0.15, 0.45, 0.035)$ and $(L, D, d_{-s}) = (488$ cm, 33.5 cm, 5 cm).

These second-mode waves propagate a distance $O(10D)$ onto the shelf before being damped to an unobservable amplitude. No second-mode waves were observed to propagate off-shelf.

Fluid velocities 20 cm before, at and 20 cm after the shelf break were measured for a set of experimental runs in which wave breaking occurred. The conditions were the same as the model comparison in figure 7. The measurements showed that the maximum on-shelf velocity in the lower layer exceeded the linear long-wave phase speed on the shelf, c_s, 20 cm before and at the shelf break. Fluid velocities greater than the local linear phase speed and the photographs which show extreme nonlinear wave steepening leading to a sharp corner in the interface suggest that the strong breaking mechanism is a kinematic instability rather than a shearing instability. The instability develops rapidly over a distance $O(D)$ and timescale $O(D/c_s)$.

The horizontal gradient in x-velocity is very large. When the velocity at the shelf

break is a maximum in the off-shelf direction, the velocity 20 cm off the shelf is nearly zero. The local vertical velocity can be estimated from the continuity equation

$$w = \int_{-h}^{z} \frac{\partial u}{\partial x}\,\mathrm{d}z \sim -\Delta u \frac{d_{-\mathrm{s}}}{\Delta x}.$$

Measurements give $\Delta u \approx -0.7c_{\mathrm{s}}$, $\Delta x \approx 20$ cm and $d_{-\mathrm{s}} = 5$ cm; therefore, $w \approx 0.18c_{\mathrm{s}}$. During the timescale of breaking, the interface would move vertically about $0.18D$ or 6 cm for the given conditions. The displacement is $O(1)$ relative to the local lower-layer depth. The resulting overturning is not surprising.

Visual observations and photographs were used to identify the presence and type (shearing or overturning) of instabilities for the complete set of experimental runs. Figure 12 shows the regions of instabilities and second-mode generation for $(-a_0/d_{-\mathrm{s}})$ *vs.* λ with $\sigma = 0.035$. Dependence on slope length is quite weak. For a fixed λ the transition from clean transmission to strong overturning is a relatively small region of weak shearing. Figure 13 is a composite of the transition region for all three density differences studied. Fewer experiments were run for $\sigma = 0.017$ and 0.053 than 0.035, so the transition regions are not as well defined. In general the results are not strongly dependent on σ or λ over the ranges examined.

In addition to the parametric regions of instabilities the amount of incident energy lost from the first mode is of interest. Some is lost to viscous stress, some energy is radiated as higher-mode waves, and the remainder contributes to local mixing in the shelf region. Estimates of energy lost from the first mode were computed as follows. The first-mode energy flux through a vertical section between time t_1 and t_2, or work W on the vertical section, is given by

$$W = \int_{t_1}^{t_2} \int_{-h}^{0} (pu + \bar{\rho}u^3)\,\mathrm{d}z\,\mathrm{d}t, \tag{5.1}$$

where p and u are the wave-induced pressure and horizontal velocity respectively and are found from the $O(1)$ continuous stratification model. By evaluating (5.1) at two locations, $W_0 = W(x_0)$ and $W_1(x_1)$, the total first mode dissipation is given by

$$D_{\mathrm{T}} = W_0 - W_1. \tag{5.2}$$

The total dissipation is made up of viscous boundary and interfacial dissipation D_{V} and dissipation due to any wave breaking D_{B} between x_0 and x_1.

For a given experimental run, W_0 and W_1, where x_0 is at the base of the slope and x_1 is the last station on the shelf, were calculated from (5.1) using the experimental measurements of $A(x, t)$ or the numerical simulations. The times t_1 and t_2 were chosen so that the complete incident wave or scattered wave group was included. Ideally, if no breaking or reflection occurs, values of (5.2) from the experimental data and the numerical simulation would be equal. With breaking, the difference would be equal to the energy lost from the lowest mode during the breaking event. Thus,

$$D_{\mathrm{B}} = W_1^{\mathrm{N}} - W_1^{\mathrm{E}}, \tag{5.3}$$

since W_0 is the same in the numerical (N) and experimental (E) calculations.

Table 3 lists average values of D_{B}, normalized by W_0, for cases with no wave instabilities and cases with strong overturning instabilities and second-mode generation for all three density differences. The results are consistent and show that in these laboratory experiments about 10 % of the incident-wave energy is lost from the lowest mode during a strong overturning instability. On average, about 40–50 % of the

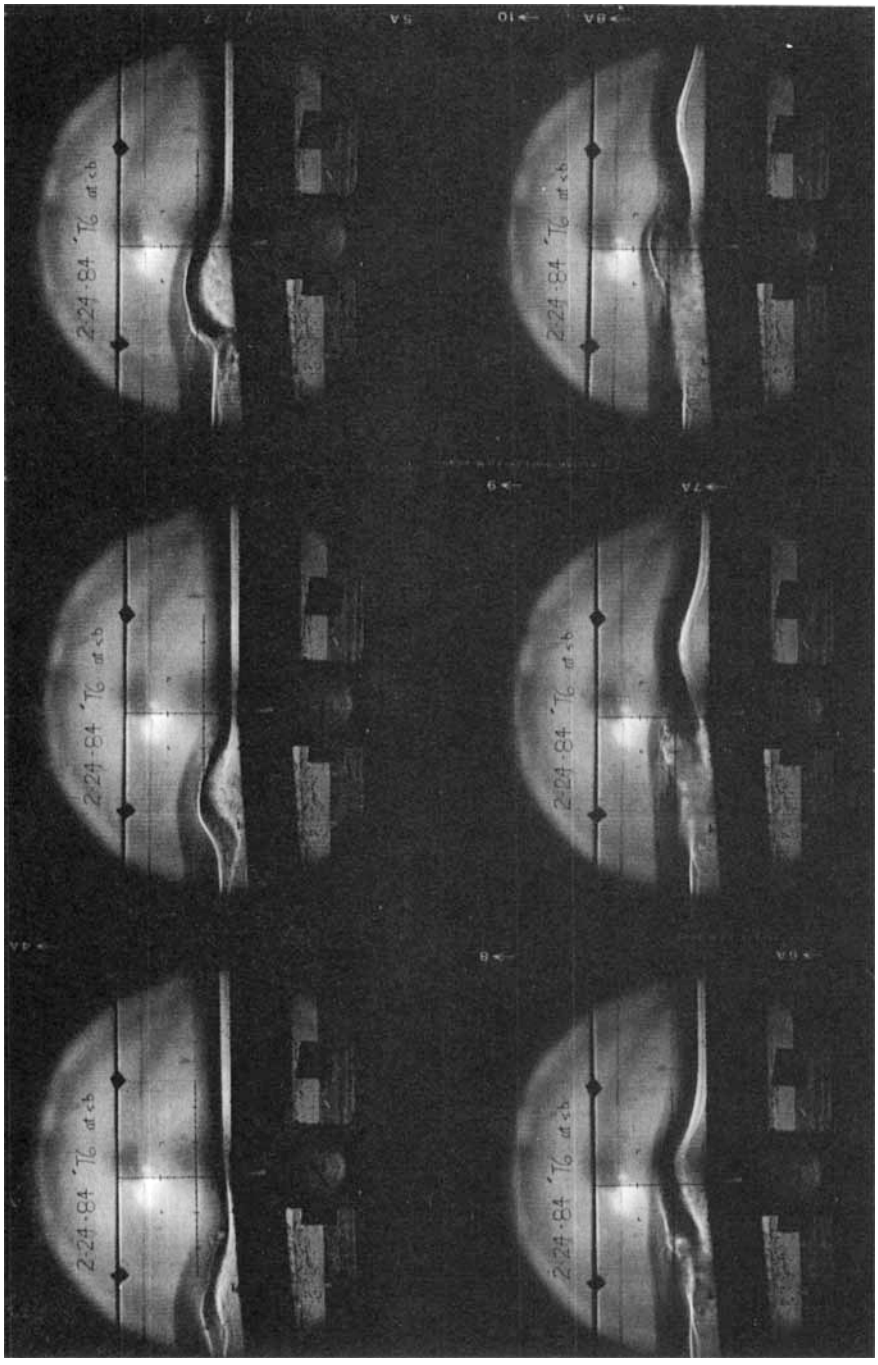
(a)
(b)
(c)
(d)
(e)
S

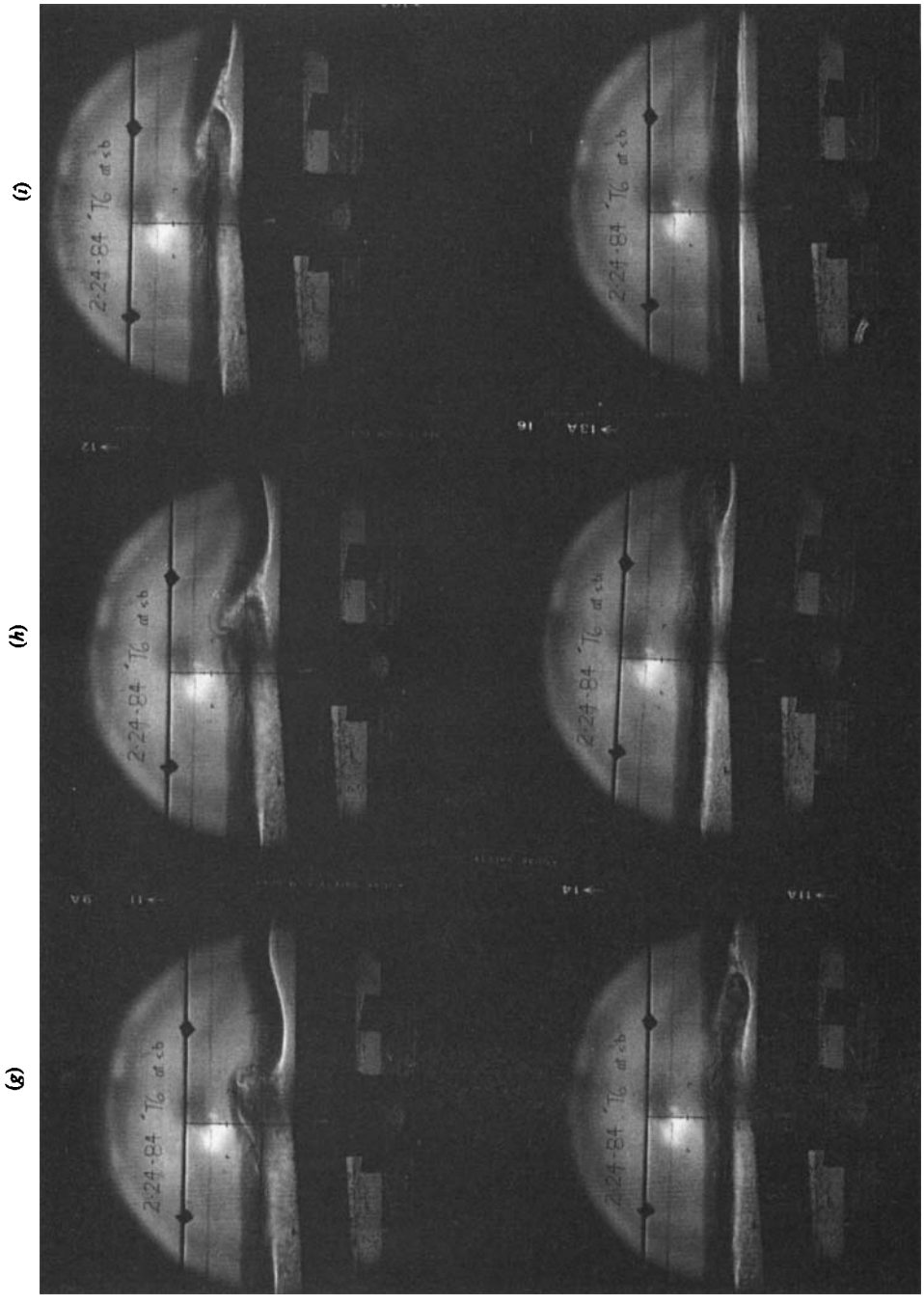

FIGURE 10. Shadowgraphs showing strong overturning event at shelf break for $(\alpha, \lambda, r, \sigma) = (-0.067, 0.29, 0.45, 0.053)$ and $(L, D, d_{-s}, c_0) = (244\text{ cm}, 33.5\text{ cm}, 5\text{ cm}, 18.7\text{ cm/s})$. (*a*) $t = 0$ (arbitrary origin); (*b*) $t = 0.9$ s; (*c*) 1.9 s; (*d*) 2.8 s; (*e*) 3.7 s; (*f*) 4.6 s; (*g*) 5.6 s; (*h*) 6.5 s; (*i*) 7.5 s; (*j*) 8.4 s; (*k*) 10.2 s; and (*l*) 22.3 s.

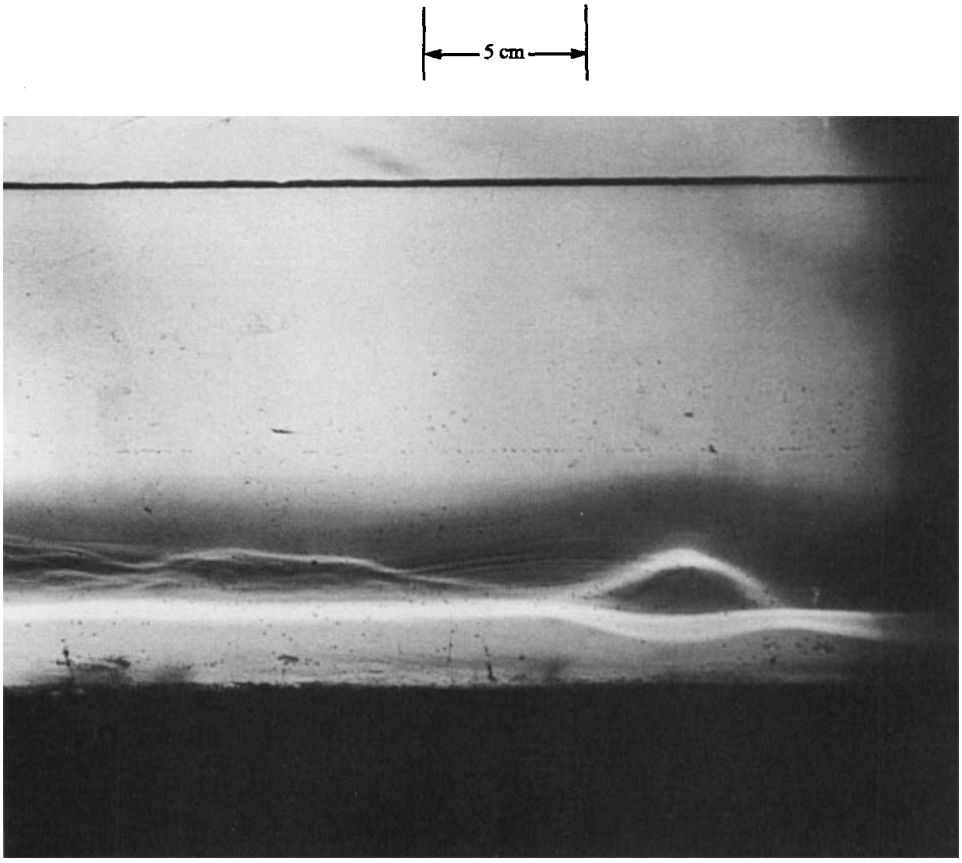

FIGURE 11. Shadowgraph 45 cm past shelf break showing second-mode wave for $(\alpha, \lambda, r, \sigma) = (-0.060, 0.15, 0.45, 0.035)$ and $(L, D, d_{-s}) = (488\text{ cm}, 33.5\text{ cm}, 5\text{ cm})$.

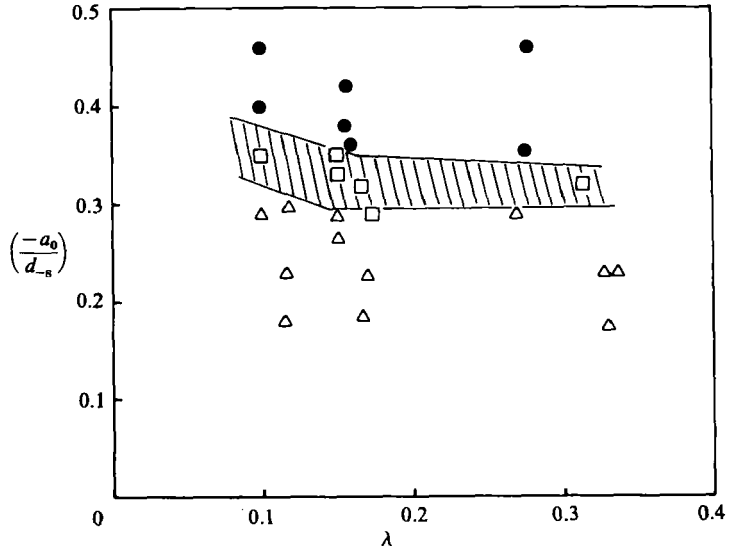

FIGURE 12. Regions of instabilities for $\sigma = 0.035$. Strong overturning and second-mode wave generation, ●; shearing, □; no instabilities, △.

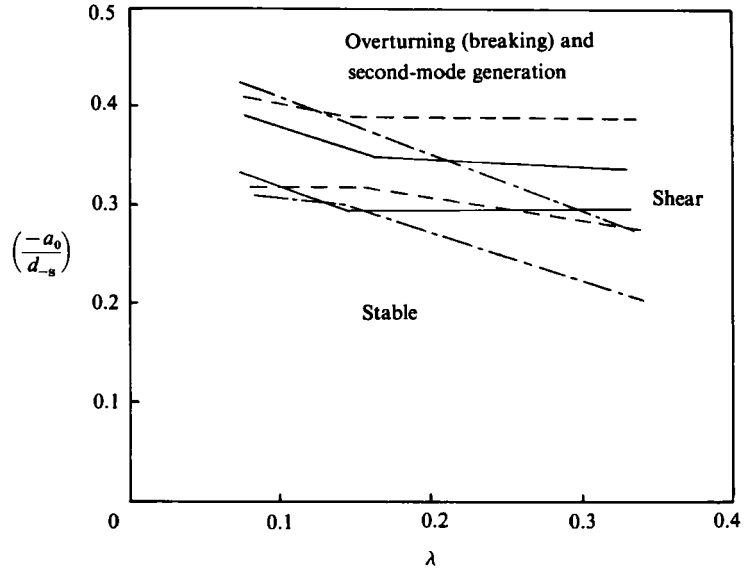

FIGURE 13. Composite of instability regions. $\sigma = 0.017$, (– – –); $\sigma = 0.035$, (——); $\sigma = 0.053$, (— – —).

$\frac{\Delta\rho}{\rho}$	(*a*) no instabilities		(*b*) strong overturning instabilities	
	Average	No. data pts	Average	No. data pts
0.017	0.05	3	0.13	1
0.035	0.00	5	0.10	4
0.053	−0.02	6	0.09	5
All runs	0.0±0.05	14	0.10±0.05	10

TABLE 3. Values of dissipation from the first mode due to breaking D_B normalized by the incident energy flux W_0 for cases with (*a*) no wave instabilities and (*b*) strong overturning instabilities

incident wave is lost to combined viscous dissipation and instabilities between $\xi = 0$ and the last measuring station so that when instabilities occur they constitute about 20 % of the total energy lost from the lowest mode.

6. Discussion

This paper has examined the evolution of single and multiple rank-ordered internal waves incident on slope–shelf topography. Specific interest has been on situations when a turning point (point of equal layer depths) is encountered on the slope. A KdV model including continuous stratification, variable depth, boundary damping and cubic nonlinearity, compared very well with experimental data over a range of stratifications, topography and wave amplitudes. In particular, cases with relatively fast slopes, exhibiting a significant reflected wave, were modelled accurately even though the theory only accounts for unidirectional propagation. Comparisons for a single solitary wave incident on slope–shelf topography were good for λ as large as

$\sim 10\alpha$. Poorest agreement was found as the lower-layer depth on the shelf was decreased and the topographic scattering increased. Errors in the amplitudes and frequencies of the tail of the scattered packet became significant, although the leading trough and scattered crests were well predicted. Comparisons for two rank-ordered incident solitary waves were good, provided $d_{-s}/d_+ > 0.5$–0.6.

It was not possible to delineate the domain of applicability of the theory any further because of laboratory constraints. The tank length prohibited examination of slope lengths much longer than the lengths tested. There would not have been enough shelf for examining the development of the scattered packet. Furthermore, the relatively strong role of viscous boundary dissipation in the laboratory would dominate the results as L increased, obscuring the roles of α and λ. Generation of clean incident solitary waves larger than those examined ($a_0/D < -0.08$) was not possible with the present wave-generation system.

Transmission of solitary waves of reversed polarity from the scattering of an incident solitary wave was not observed in any of the experiments. In an inviscid system, transmission is possible for $\lambda < |\alpha|$ and the number and amplitudes of solitary wave transmitted increases as λ decreases for fixed α (Helfrich *et al.* 1984). Numerical experiments including dissipation, however, show that transmission depends on the relative influence of damping and topography. At laboratory scale, damping, combined with relatively fast slopes, is strong enough to completely dissipate any weak waves of reversed polarity which could emerge asymptotically in an equivalent inviscid system. In the ocean, damping plays a less important role than in the laboratory and transmission of waves of reversed polarity is possible.

Weak shearing and strong breaking-wave instabilities were observed in the neighbourhood of the shelf break and empirical stability boundaries were defined. Comparisons of the theoretical model with experiments exhibiting strong breaking were surprisingly good even though the events are strongly nonlinear and the model does not account for wave instabilities. The experiments also illustrated a mechanism of lowest-mode instability which led to significant vertical and horizontal mixing and apparent second-mode solitary-wave generation. Large second-mode solitary waves may have closed streamlines, and therefore transport mixed fluid (Davis & Acrivos 1967; Maxworthy 1980). Although entrapment of mixed fluid was not positively identified in this study, the possibility of mass transport and the modification of the stratification by internal wave breaking may be significant and is worthy of further study (cf. Pingree & Mardell 1981).

Use of the theoretical model to study actual oceanographic situations should be straightforward; however, several questions arise. The first concerns the boundary layers. In the laboratory, boundary damping is laminar and the model correctly accounts for this process. In the field the boundary damping will be turbulent. In order to use the model an effective turbulent eddy viscosity must be specified. This is not completely satisfactory since the concept is heuristic and *a priori* estimates of eddy viscosity, dependent to some degree on wave parameters, are difficult to make. Since boundary damping is less important in the field than in the laboratory, use of an eddy viscosity, found perhaps by calibration, should not obscure analysis of other features of model comparisons with field data.

Values of λ (the slope-length parameter) for oceanic conditions can be smaller than the range examined in the experiments (cf. table 1). This is not anticipated to be a problem in application of the model. As λ decreases the influence of the variable topography on wave evolution decreases. This work has shown that the theory gives very good results for λ in the range $O(\alpha$–$10\alpha)$ and Koop & Butler (1981) and Segur

& Hammack (1982) have demonstrated good agreement between KdV theory and experiment in constant depth ($\lambda = 0$).

Oceanic observations often show wave amplitudes which might not be considered weakly nonlinear if the pycnocline depth, rather than the total depth, is used as the amplitude normalization scale. From table 1 the Andaman Sea and Massachusetts Bay data have values of $a_0/d_+ = 0.16$ and 0.33 respectively. Both cases might no longer be considered weakly nonlinear. The point at which a weakly nonlinear theory is no longer valid is not easily defined theoretically, but comparisons with experiments serve to identify domains of validity. Koop & Butler (1981) and Segur & Hammack (1982) found good agreement between first-order KdV theory and measured internal-solitary-wave characteristics in constant depth for $a_0/d_\pm$ as large as 0.2. Adopting this amplitude scaling, the results of this study for variable depth gave good results for a_0/d_+ as large as 0.25. Moreover, very good agreement between theory and experiment was observed in the shelf-break region where the wave amplitudes were quite large and the dynamics are certainly not weakly nonlinear.

Application of the laboratory breaking criteria to oceanographic scales should be possible owing to the kinematic nature of the instability. However, care must be taken that field conditions lie inside the parameter range of figures 12 and 13. It is not clear that the weak dependence of the instability regions on λ will continue for $\lambda < 0.1$. Clearly the dynamical results of the breaking in the laboratory are scale dependent and may not apply to oceanographic situations.

We wish to thank Professor David Benney for helpful discussions on the evolution equations and Jack Crocker for building experimental equipment. This work was supported by a contract with the Office of Naval Research (Coastal Sciences).

REFERENCES

Apel, J. R. & Holbrook, J. R. 1983 The Sulu Sea internal soliton experiment, Part A: overview and satellite data. Contribution no. 596 from PMEL/NOAA.

Benjamin, T. B. 1967 Internal waves of permanent form in fluids of great depth. *J. Fluid Mech.* **29**, 559–592.

Davis, R. E. & Acrivos, A. 1967 Solitary internal waves in deep water. *J. Fluid Mech.* **29**, 593–607.

Farmer, D. M. & Smith, J. D. 1980 Tidal interaction of stratified flow with a sill in Knight Inlet, *Deep-Sea Res.* **27 A**, 239–254.

Fornberg, B. & Whitham, G. B. 1978 A numerical and theoretical study of certain nonlinear wave phenomena. *Phil. Trans. R. Soc. Lond.* A **289**, 373–404.

Fu, L. L. & Holt, B. 1982 Seasat views oceans and sea ice with synthetic aperature radar. *JPL Publication* 81-120, Feb. 15.

Gear, J. A. & Grimshaw, R. 1983 A second order theory for solitary waves in shallow fluids. *Phys. Fluids* **26**, 14–29.

Grimshaw, R. 1981 Evolution equations for long, nonlinear internal waves in stratified shear flows, *Stud. Appl. Maths* **65**, 159–188.

Giese, G. S., Hollander, R. B., Fancher, J. E. & Giese, B. S. 1982 Evidence of coastal seiche excitation by the tide generated internal solitary waves. *Geophys. Res. Lett.* **9**, 1305–1308.

Goring, D. G. 1978 Tsunamis – The propagation of long waves onto a shelf, *W. M. Keck Lab. Rep.* KH-R-38. California Institute of Technology, Nov.

Halpern, D. 1971 Observations of short period internal waves in Massachusetts Bay. *J. Mar. Res.* **29**, 116–132.

Haury, L. R., Briscoe, M. G. & Orr, M. H. 1979 Tidally generated internal wave packets in the Massachusetts Bay. *Nature* **278**, 312–317.

HELFRICH, K. R. 1984 On long nonlinear internal waves over topography. Ph.D. thesis, Dept. of Civil Engineering, MIT.

HELFRICH, K. R., MELVILLE, W. K. & MILES, J. W. 1984 On interfacial solitary waves over slowly varying topography. *J Fluid Mech.* **149**, 305–317.

KAKUTANI, T. & MATSUUCHI, K. 1975 Effect of viscosity on long gravity waves. *J. Phys. Soc. Japan* **39**, 237–246.

KAKUTANI, T. & YAMASKI, N. 1978 Solitary waves on a two-layer fluid. *J. Phys. Soc. Japan* **45**, 674–679.

KOOP, C. G. & BUTLER, G. 1981 An investigation of internal solitary waves in a two-fluid system. *J. Fluid Mech.* **112**, 225–251.

LEE, C.-Y. & BEARDSLEY, R. C. 1974 The generation of long nonlinear internal waves in a weakly stratified shear flow. *J. Geophys. Res.* **79**, 453–462.

LEONE, C., SEGUR, H. & HAMMACK, J. L. 1982 The viscous decay of long internal solitary waves. *Phys. Fluids* **25**, 942–944.

LIU, A. K., APEL, J. R. & HOLBROOK, J. R. 1984 Nonlinear internal wave evolution in the Sulu Sea. *Dynamics Technologies Rep.* DT-8305-01.

LONG, R. R. 1953 Some aspects of the flow of stratified fluids I. A theoretical investigation. *Tellus* **5**, 42–58.

LONG, R. R. 1956 Solitary waves in one- and two-fluid systems. *Tellus* **8**, 460–471.

MADSEN, O. S. & MEI, C. C. 1969 The transformation of a solitary wave over an uneven bottom. *J. Fluid Mech.* **39**, 781–791.

MAXWORTHY, T. 1979 A note on internal solitary waves produced by tidal flow over a three-dimensional ridge. *J. Geophys. Res.* **84**, 338–346.

MAXWORTHY, T. 1980 On the formation of nonlinear internal waves from the gravitational collapse of mixed regions in two and three dimensions. *J. Fluid Mech.* **96**, 47–64.

MILES, J. W. 1976 Korteweg de Vries equation modified by viscosity. *Phys. Fluids* **19**, 1063.

MILES, J. W. 1979 On internal solitary waves. *Tellus* **31**, 456–462.

MILLER, G. R. 1966 The flux of tidal energy out of the deep oceans. *J. Geophys. Res.* **71**, 2485–2489.

MYERS, J. J., HOLM, C. H. & MCALLISTER, R. F. 1969 *Handbook of Ocean and Underwater Engineering*. McGraw-Hill.

OSBORNE, A. R. & BURCH, T. L. 1980 Internal solitons in the Andaman Sea. *Science* **208**, 451–459.

PEARSON, H. J. & LINDEN, P. F. 1983 The final stage of decay of turbulence in a stably stratified fluid. *J. Fluid Mech.* **134**, 195–203.

PINGREE, R. D. & MARDELL, G. T. 1981 Slope turbulence, internal waves and phytoplankton growth at the Celtic Sea shelf-break, *Phil. Trans. R. Soc. Lond.* A **302**, 663–682.

SANDSTROM, H. & ELLIOTT, J. A. 1984 Internal tide and solitions on the Scotian Shelf: a nutrient pump at work. *J. Geophys. Res.* **89**, 6415–6426.

SEGUR, H. & HAMMACK, J. L. 1982 Soliton models of long internal waves. *J. Fluid Mech.* **118**, 285–304.

THORPE, S. A. 1971 Asymmetry of the internal wave seiche in Loch Ness. *Nature* **231**, 306.

THORPE, S. A. 1978 On the shape and breaking of finite amplitude internal gravity waves in a shear flow. *J. Fluid Mech.* **85**, 7–32.